

Ring conformations in bidisperse blends of ring polymers

M. Lang¹

January 6, 2022

¹Leibniz Institut für Polymerforschung Dresden, Hohe Straße 6, 01069 Dresden, Germany.

Abstract

The size of rings (also called cyclic polymers) in bidisperse blends of chemically identical rings is analyzed by computer simulations. Data of entangled ring blends and blends of interpenetrating rings are compared and it is shown that the compression of entangled rings can be explained by the changes in the penetrable fraction of the minimal surface bounded by the ring. Corrections for small rings can be approximated by a concatenation probability $1 - P_{OO}$ that a ring entraps at least one other ring. Both results are in line with a previous work [1] to explain the compression of entangled rings in monodisperse melts. Bond-bond correlations in melts of interpenetrating rings lead to similar corrections for ring sizes as reported previously [2] for monodisperse linear melts. For entangled rings, bond-bond correlations show an anti-correlation peak at a curvilinear distance of about ten segments that coincides with a horizontal tangent in the normalized mean square internal distances along the ring. Both observations become independent of melt molecular weight for sufficiently large degrees of polymerization and such behaviour is not found in samples with entanglements switched off. In consequence, the length scale of topological interactions (entanglement length) in a melt of entangled rings must be considered as constant in contrast to a recent proposal by Sakaue [3].

1 Introduction

Recently, it was suggested [1] that the conformations of non-concatenated rings in monodisperse melt may follow four different regimes as function of the degree of polymerization N . These regimes are separated by three characteristic degrees of polymerization, N_{OO} , N_C , and N^* . N_{OO} describes the onset of the effect of non-concatenation below which topological effects are not important, N_C is the cross-over between weak and strong compression of rings, and N^* is defined by the cross-over from a non-concatenation contribution $f_n \sim \phi R^2$ to an overlap dominated concatenation contribution $f_n \sim \phi N^{1/2}$ at $N > N^*$.

Below N_{OO} , the rings are uncompressed and ring conformations nearly ideal. For $N_{OO} < N < N_C$, ring polymer conformations may be described by a free energy of form

$$\frac{\Delta F}{kT} \approx b\phi R^2 + v_e \frac{N^2}{R^3}. \quad (1)$$

Here, the first term with polymer volume fraction ϕ and root mean square bond length b counts the number of rings that need to be expelled from the gyration volume of a given ring. This contribution was conjectured [1] by an analysis of the number of concatenated states in a melt of interpenetrating rings. The second term describes the effect of topology in analogy to excluded volume [4], which should be the best approximation for the weakly compressed rings of the present study (cf. section 4 and ref [1]). The cross-over to strong compression at N_C is characterized by the transition to a dominating third virial contribution $\sim b^6 N^3/R^6$ that replaces the second term in equation (1) for $N > N_C$ as proposed by Grosberg [5]. A normalization constant v_e for entangled strands is introduced in equation (1) in analogy to the excluded volume for entanglements. The equilibrium ring size is, thus, obtained as

$$R \sim N^{2/5} (\phi b/v_e)^{-1/5}. \quad (2)$$

Above N^* , the number of rings that needs to be expelled is controlled by the number of overlapping rings $\sim b^3 N/R^3$, since $b\phi R^2$ cannot become larger than the number of overlapping rings. Compression is in both cases balanced by a term $\sim b^6 N^3/R^6$. This yields ring sizes $R \sim bN^{3/8}$ for $N_C < N < N^*$ and $R \sim bN^{4/9}$ for $N > N^*$.

In the present work, we focus on bidisperse blends of ring molecules at $N < N_C$ in order to clarify differences between previous theoretical works [1, 3, 6, 7]. The idea behind this procedure is that the majority species of rings determines the properties of the melt. Therefore, inserting a small amount of minority rings of different molecular weight into a melt of chemically identical rings probes the properties of the surrounding melt and the topological interactions between the rings. This is of particular importance, since the models of Cates and Deutsch [6], Sakaue [3, 7], or Lang *et al.* [1] implicitly or explicitly predict different behaviours in bidisperse blends. While the first can only be extended to have an onset of compression for melt molecular weight $\sim N^{1/2}$, the second model requires the topological length scale (entanglement length) to be decreasing for increasing molecular weight. The third model assumes that the density of entanglements is independent of N for constant ϕ beyond the onset of the effect of topology at the concatenation length N_{OO} .

In addition to the compression of rings in entangled melts of large $b\phi R^2$ it is expected that the same principles as for linear chains hold for the swelling of entangled rings in low molecular weight rings. Let M denote the degree of polymerization of the majority species that dominates the melt properties and N denote the degree of polymerization of a chemically identical fraction of chains that is dilute in the melt of M -mers. For linear chains, this situation is typically discussed [8, 9] by using a Flory ansatz of the form

$$\frac{\Delta F}{kT} \approx \frac{v}{M} \frac{N^2}{R^3} + \frac{R^2}{b^2 N}, \quad (3)$$

which balances the excluded volume contribution with the deformation of an ideal chain. Here, $v \approx b^3$ is the excluded volume per monomer. Equilibrium conformations are characterized by

$$R \sim bN^{3/5} M^{-1/5}. \quad (4)$$

The onset of swelling is found by equating $N^{1/2} = N^{3/5}M^{-1/5}$, which yields a matrix molecular weight $M_c \sim N^{1/2}$ to cross over between swollen and nearly ideal conformations of the N -mers.

In recent years, it was shown that bond-bond correlations introduce corrections to the scaling of the size of linear chains [2, 10]. Furthermore, one would expect that entanglement effects set in at some degree of polymerization proportional to the entanglement degree of polymerization N_e . Since M_c is a function of N , both regimes can overlap while simultaneously being perturbed by these bond-bond correlations making a clean analysis quite problematic. In order to circumvent such difficulties, two series of blends of bidisperse rings were created which differ only by the fact that in one series the topology of the rings is fixed because entanglements are active (called “entangled” or “non-interpenetrating” samples), while for the other series entanglements are switched off and excluded volume is maintained (“interpenetrating” samples). It is expected that the samples without entanglements show swelling and related corrections in melt [2, 10] similar to linear chains, a hypothesis that is successfully tested below. In conclusion, a comparison between both cases then allows for a rather direct determination of the effect of topology onto ring conformations.

The paper is structured as follows: Section 2 describes the simulation method and parameters of the simulations. Section 3 specifies the properties of the (minimal) surface that is spanned by a ring polymer and the relation to the total number of rings in topological conflict is explained. This analysis is fundamental for understanding concatenation, since each concatenated ring must cross the surface that is bounded by the ring. The internal structure of the rings is compared with the available models in literature [1, 3, 6, 7] in section 4 and it is shown that interpenetrating rings show the same scaling and corrections due to excluded volume as linear chains in melts. The sizes of interpenetrating and entangled rings are compared in section 5 and all results are summarized in section 6.

2 Simulation method and samples

As in the preceding work [1], we use the bond-fluctuation model (BFM) [11] to simulate bidisperse blends of ring polymers. In this method, each monomer is represented by a cube occupying eight lattice sites on a cubic lattice. In the standard definition of this algorithm, the bonds between monomers are restricted to a set of 108 bond vectors which ensure cut-avoidance of polymer strands by checking for excluded volume. Monomer motion is modeled by random jumps to one of the six nearest lattice positions. A move is accepted, if the bonds connecting to the new position are still within the set of bond vectors and if no monomers overlap. All samples of the present study were created in simulation boxes of 128^3 lattice sites with periodic boundary conditions at occupation density $\phi = 0.5$.

In the present work, we use this method to create blends of non-concatenated rings. Additionally, we perform simulations where we allow for an extended set of bond vectors as described in [12] such that all entanglements are switched off, while excluded volume interactions are mainly unaffected. In consequence, the rings can interpenetrate each other to form concatenated conformations. In both

cases, relaxation of the rings was monitored by the autocorrelation function of the vectors connecting opposite monomers of a ring. All samples were relaxed several relaxation times of the longest rings in the bidisperse blends. Afterwards, chain conformations were analyzed from snapshots of the ring solutions from a very long simulation run. The error of the data points is computed by the total number of statistically independent conformations available.

For the present study, we prepared bidisperse solutions of entangled rings with a fraction of 1/32 of minority species with degree of polymerization $N = 2^i$ in melts of $M = 2^j$ monomers, whereby i and j are all integers with $6 \leq i \leq 10$ and $4 \leq j \leq 10$. A second series of interpenetrating rings with 1/32 fraction of $N = 2^i$ and $6 \leq i \leq 9$ was prepared in the same range of melt degrees of polymerization (except of skipping some of the largest M for the smallest two N as indicated in the Figures). All samples containing $N = 1024$ were run for 10^9 Monte Carlo Steps (“MCS”: attempted moves per particle), the samples with $N = 512$ for 5×10^8 MCS, and all other samples for at least 10^8 MCS after equilibration. The data below represent averages as determined over the full simulation runs.

3 The minimal surface of a ring polymer

Consider a circular random walk made by a randomly coiled wire. Dipping this ring into a bowl of suds and removing it afterwards, one typically observes the formation of a thin layer of suds held by the ring contour that optimizes its area by surface tension. This simple experiment determines the minimal surface bounded by the ring. The basic idea of the model in reference [1] is that the (minimal) surface spanned by the ring contour can be used to estimate the number of topological conflicts among overlapping rings, since any concatenated conformation has to pass through the area bounded by the ring, see the upper part of Figure 1. The minimal property of this surface was originally chosen by convenience, since concatenation can be detected by any surface bounded by the ring. However, the minimal surface is the only uniquely defined surface - to the knowledge of the author - that is in any possible situation inside the volume spanned by the ring. Thus, crossing the minimal surface is always equivalent to overlap *and* possible concatenation, which simplifies the discussion below. Therefore, the minimal surface will be used in the present chapter to demonstrate that rings in melts reduce the fraction of the bounded area that can be penetrated or concatenated for avoiding concatenated states in melts of non-concatenated rings. However, we have to keep in mind that the minimal surface is only a concept to properly count or estimate the number of possible concatenated states per ring but it is solely the number fraction of concatenated vs. not concatenated states (and not the minimal surface) that drives the compression of non-concatenated rings in melts.

In reference [1] it was assumed that a rather constant fraction of all conformations that intersect with the minimal surface produces a concatenated state. This assumption should be a reasonable approximation as long as the root mean square length of the intersecting walk is comparable or larger than the distance between intersection point and boundary of the minimal surface. The

observed good agreement of the results for monodisperse melts of rings with the estimate based upon the minimal surface corroborates this simplifying assumption. But this simplification clearly deserves revision for mixtures of rings with a broad distribution of ring sizes. Due to the limited range of molecular weights above N_{OO} within the present study, this discussion is not necessary and thus, must be postponed to a future work. In consequence of this simplification, we further can assume an approximately constant concatenation probability as function of the distance to the boundary of the minimal surface for the samples of the present study. Within this approximation, the area distribution of the minimal surface can be interpreted as distance distribution of possible concatenations with respect to the boundary of the ring.

In polymer physics, the tube model is typically used to model the effect of entanglements of overlapping polymer strands [13]. In this model, it is assumed that the entanglements along the contour of a chain confine the motion of the chain into a tube like region in space and thus, predominantly the strands in contact with a given molecule control the polymer dynamics. The situation is different for the conformations of non-concatenated rings in melt. Any conformation that would be concatenated needs to be expelled out of the volume of a given ring, independent of the position of the concatenation with respect to the ring contour. This difference is sketched in the lower part of Figure 1. Therefore, any model (like the tube model) that neglects concatenations in the inner part of the (minimal) surface is not suitable to learn about ring conformations. Conversely, the topological approach of the present work is also not suitable to learn about the dynamics of the rings, because all entangled strands that are not part of concatenated conformations are not detected in our analysis and thus, would not be taken into account to estimate the dynamics of the ring.

To the knowledge of the author, the problem of the minimal surface of a closed random walk is unsolved and it will not be attempted to rigorously derive its properties. Knotted rings can be related to Seifert-surfaces [14], but due to the fact that the knotting length [1] is larger than the largest degree of polymerization in our study, we ignore the effect of knotting for the remainder of this work. Unknotted random walks bound much simpler surfaces: the bounded area of an unknotted random walk is always homeomorph to a circular disc [14]. But the shape of this bounded area in space is highly non-trivial.

In order to gain some insight into the properties of the minimal area bounded by a ring polymer, an algorithm for the triangulation of the area spanned by a ring was developed. Some steps of this triangulation are shown in Figure 2. The total area was subdivided into $6N$ triangles using N joints along the ring and inserting N additional points at the middle of each segment. Further $2N - 2$ mobile junctions are placed inside the area such that for each generation of mobile junctions from boundary inwards the number of junctions is divided by two. Each new junction is coupled to three junctions of the previous generation and the next neighbors of the same generation. Afterward, the total area of the surface is optimized by randomly displacing one of the $2N - 2$ inner mobile junctions using a Metropolis [15] algorithm for the change in area while quickly driving the “temperature” to zero. Optimization was stopped, if five consecutive cycles over all mobile junctions did not further

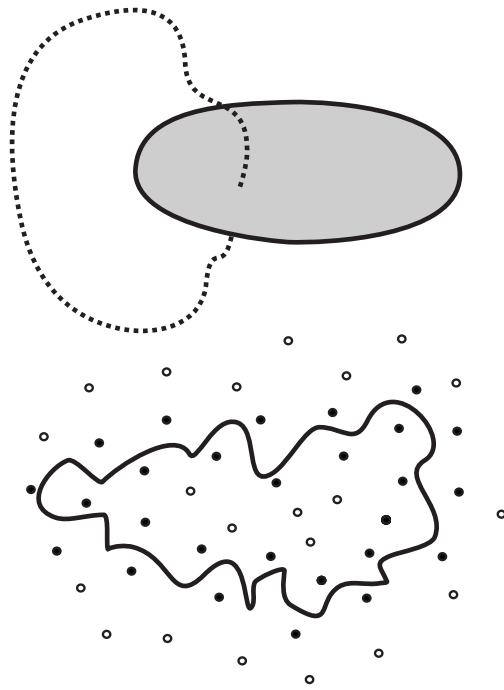


Figure 1: Upper Figure: concatenated conformations (dashed line) intersect with the minimal surface of the overlapping ring (grey color). Lower Figure: a different fraction of overlapping strands is important for dynamics as compared to conformations: the entanglements along the ring contour (full dots) inside and outside of the ring for dynamics, and all entangled strands (full and open dots) inside the ring contour for conformations.

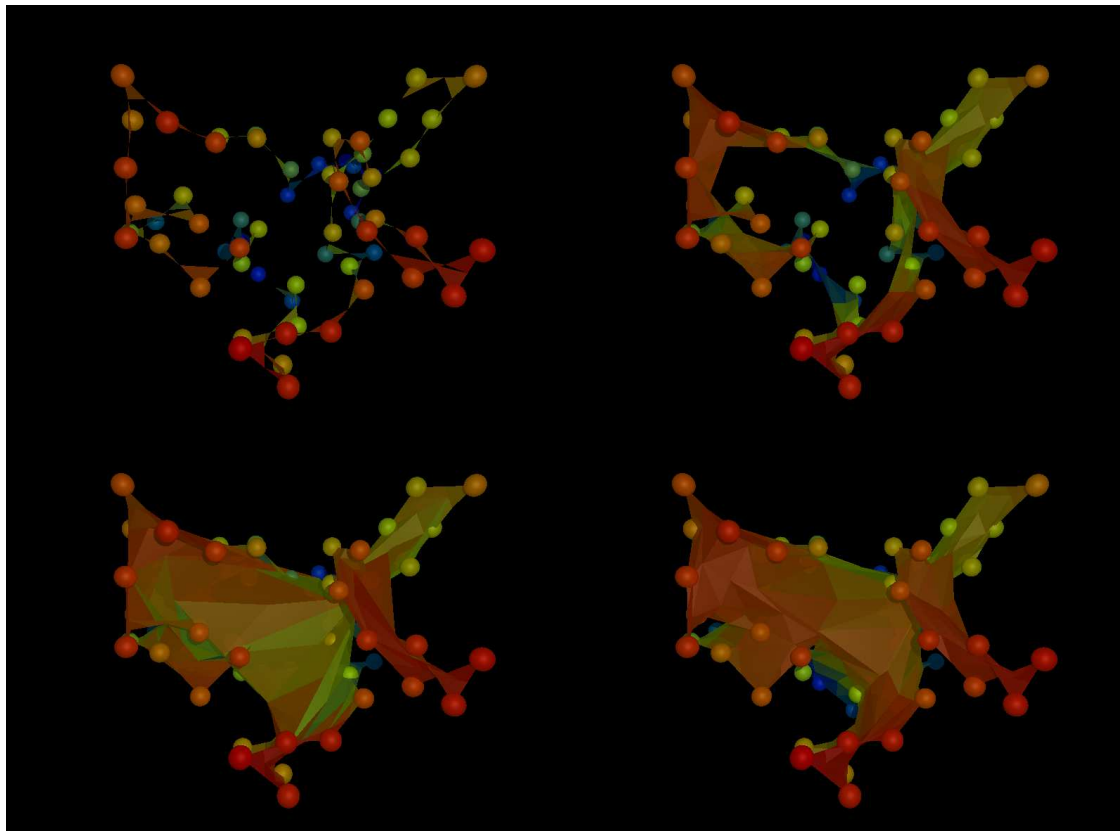


Figure 2: (All figures: color online) Left top: A (closed) random walk and the first step of triangulation. Beads display monomers, the color of the beads changes from red (closest bead) to blue (most distant beads). Same color code applies for triangles and is determined by the centers of mass of triangles. Bead size is $1/4$ of the size in simulation to make the area along the boundary visible. Right top: the first four generations of triangles (second generation of mobile junctions) form a band along the ring contour of roughly b width with the inner area of the ring still uncovered. Left bottom: full triangulation prior to optimization of area. Right bottom: fully optimized area

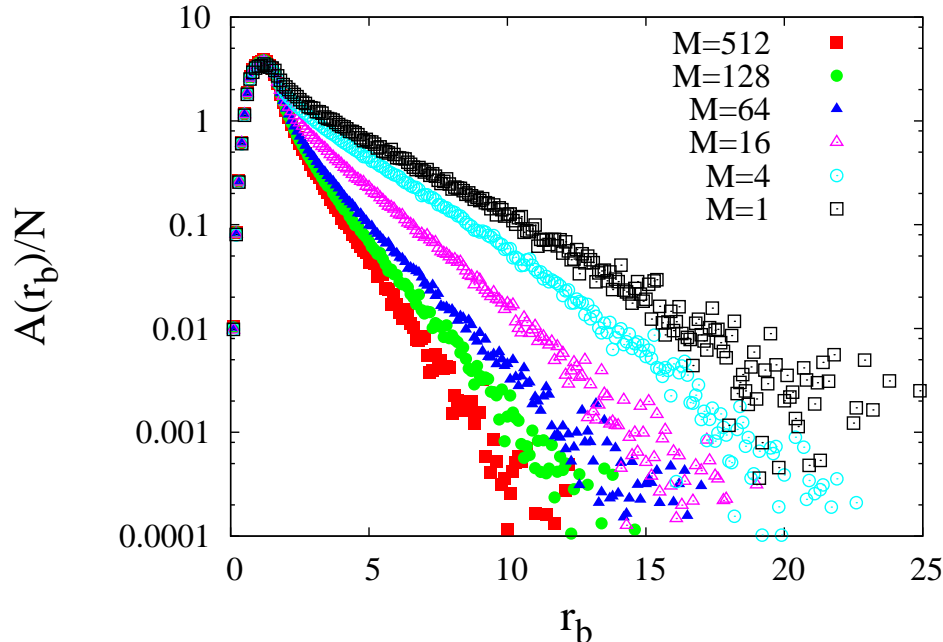


Figure 3: Area A per bond as function of the minimum distance r_b to the boundary for a series of ring polymers with $N = 512$ monomers in melts of M monomers. The length unit is the length unit of the simulation lattice as in all Figures below.

minimize the area. This rapid cooling protocol was tested against a slow minimization and shown to lead to an inaccuracy of approximately 1% as compared to the best results. Note that such a rapid cooling scheme and this rather coarse triangle mesh were necessary to be able to analyze all available ring conformations. After minimization, the area of each triangle was computed and the area analyzed as function of the distance between the center of mass of the triangle and the nearest ring monomer. The results are discussed in the following paragraphs.

The results for a series of entangled samples with long N -mers of 512 monomers in melts of rings of M monomers is shown in Figure 6. Here, r_b is the minimum distance of the center of mass of an area segment to the nearest monomer of the ring. All data show a peak at $r_b \leq 2$ and an exponential decreasing area as function of $r_b > 2$. Note that a monomer in the simulations has a diameter of 2 lattice units and thus, the minimum distance of area sections that can be penetrated is $r_c = 2$. The data overlap in the region of the peak, while the exponential decrease depends clearly on the molecular weight of the surrounding melt. Note that the samples $M < 16$ refer to swollen rings and $M > 16$ to compressed rings, while $M = 16$ is close to being ideal (up to corrections to screening, as discussed later). Figure 6 clearly demonstrates that rings change their conformations upon swelling or compression such that mainly area sections with large distance to the boundary are created or destroyed. The area along the boundary remains mainly unmodified.

In order to understand the exponential tail of the area distribution it is attempted to search for scaling variables that lead to a collapse of the data. The simplest expectation is to assume that the

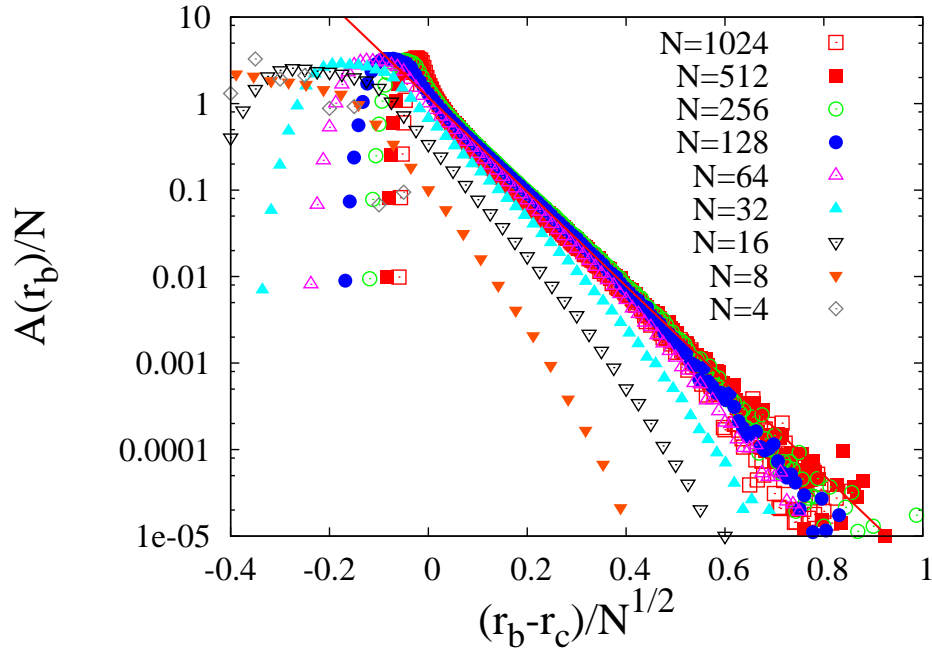


Figure 4: Area A per bond as function of the minimum distance r_b to the boundary for a series of freely interpenetrating monodisperse melts of rings of N monomers. The line indicates an exponential decay.

distance to the central sections of the minimal surface might scale as the diameter of the ring, which is $\sim N^{1/2}$ for the freely interpenetrating rings. In order to test this hypothesis, the area distribution of a series of freely interpenetrating ring melts is plotted in Figure 4 vs $(r_b - r_c)/N^{1/2}$, which collapses the data for sufficiently large N . The same collapse is obtained for the data of sufficiently large swollen rings in monomeric solvent when using the same cut-off r_c and the corresponding power of $\nu \approx 0.588$ [16], as demonstrated in Figure 5.

Figure 6 shows that the ring area of entangled melts of rings is reduced quicker than the total size of the ring: instead of for $N^{2/5}$, a best overlap of the data at large N is found for $(r_b - r_c)/N^{1/3}$. This difference suggests that a reduction in area for preventing penetration might drive the compression of the rings. The total area for penetration is of order $N^{4/3}$ and thus, still an increasing function of N . Therefore, penetrations of double folded sections of overlapping rings are clearly reduced as compared to interpenetrating melts, but are not fully excluded for large N . This is a crucial point for understanding the dynamics of melts of rings and deserves a more detailed investigation in a forthcoming work.

Figures 3 to 6 suggest that a cut-off of $r_c \approx 2$ at $\phi = 0.5$ defines the onset of the exponential tail of the area distribution¹. The area very close to the boundary $r_b < 1$ cannot be distinguished from the effect of excluded volume and is not accessible to neither bonds nor monomers nor it can be adjusted by creating double folds. Therefore, the area at $r_b < 1$ is expected to remain constant

¹Note that r_c should scale as the blob size in semi-dilute solutions of rings.

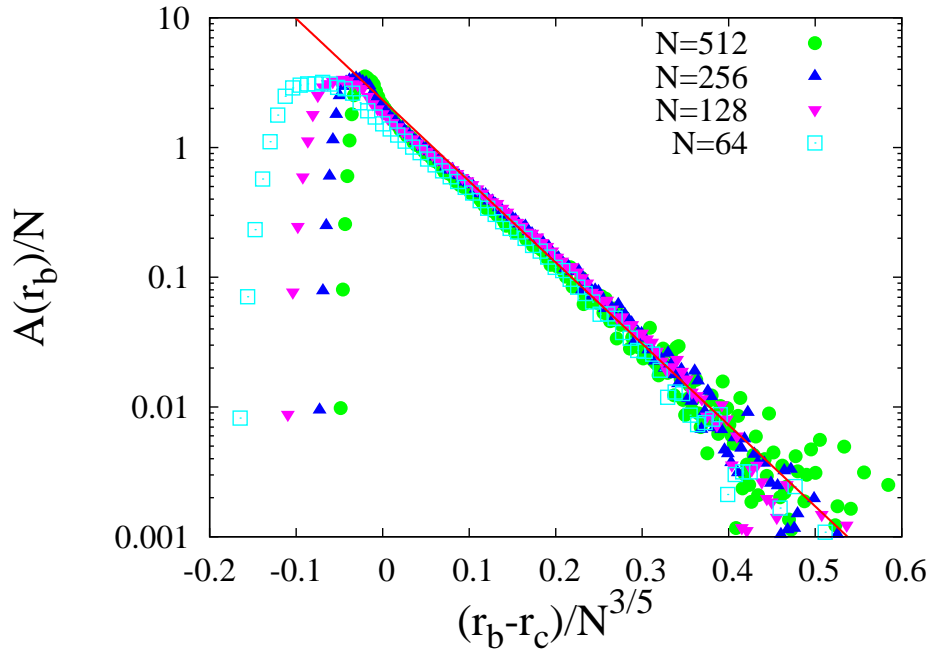


Figure 5: Area A per bond as function of the minimum distance r_b to the boundary for a series of fully swollen non-knotted non-concatenated rings in monomeric solvent.

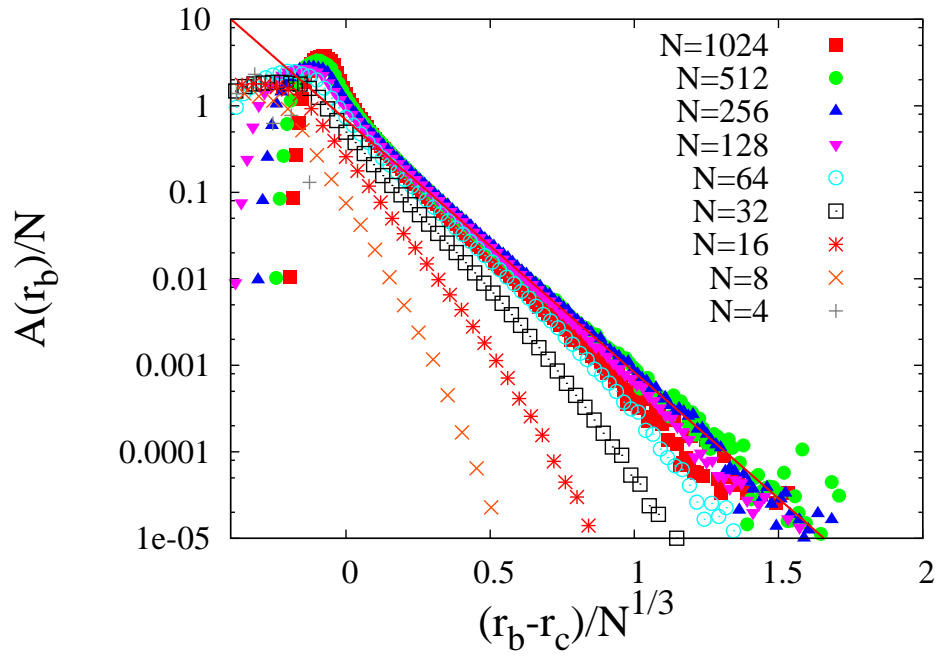


Figure 6: Area A per bond as function of the minimum distance r_b to the boundary for a series of monodisperse, entangled rings in melt.

as function of N . The area at distance $1 < r_b \lesssim 2$ lattice units is subject to local conformational changes or self contacts but not to penetration by other rings. Penetration requires a minimum area diameter of ≈ 4 lattice units, since the monomer diameter is two lattice units.

The exponential tail $\sim \exp(-a(r_b - r_c)/N^{1/2})$ in Figure 3 at $r_b > 2$ implies a correction $\sim N^{1/2}$ to scaling leading a total area of order $R^2 N^{1/2}$. The number of monomers of an overlapping ring of same degree of polymerization N in contact with the minimal surface is of order $\sim N^{1/2}$. Thus, the number of rings that have to be expelled is $f_n \sim R^2$, as found previously in ref. [1]. However, there is a more subtle point missing in this discussion: an inner area $\sim R^2 N^{1/2}$ is equivalent to a volume of order R^3 due to $R \sim N^{1/2}$ for random walks. Furthermore, a scaling of the inner area $\sim R^2 N^{1/2}$ is only possible, if the average curvature of the minimal surface is rather independent of N . The point is that sufficiently small sections of the inner area appear locally flat as long as the size of the area is below the curvature radius of the minimal surface. Larger areas fully cover space and the number of returns of a second random walk to this curved area becomes $\sim N$. If this is the case, the total number of excluded rings becomes $\sim R^2 N^{-1/2}$, which is $\sim N^{1/2}$ and, thus, proportional to the overlap number. According to the fraction of overlapping pairs of rings that mutually would entangle each other, this is expected in the limit of very large N above a critical degree of polymerization N^* [1] that is beyond the largest degree of polymerization in the present study. Finally, since semi-dilute solutions of polymers can be described by a melt of blobs, rescaling N by the number g of monomers in a blob brings us back to the above estimate in melts, since both bounding rings and penetrating rings are rescaled by the same g . Altogether, the inner part of the area leads to a penalty for non-concatenation $\sim \phi R^2$ as introduced in ref [1], since the density of surrounding rings is $\sim \phi$.

The resulting picture for the minimization of the bounded area for $N \leq 1024$ of the present study can be discussed by using the data of Figure 7. The lines in Figure 7 serve merely as a test of consistency of the above analysis. Note that a test with a limited number of rings but a finer mesh for triangulation showed that the absolute contribution of the different sections of the area are slightly modified with increasing number of triangles, but the function describing the form of the contributions is merely unchanged. First, the fraction of the area at $r_b < 1$ remains mainly constant, as explained above. Up to $N \approx 100$, the fraction of area close to the boundary $A(1 < r_b < 2)$ that is subject to self-contacts and local unfolding of rings is increasing in Figure 7 and getting approximately constant for large N . As mentioned above, this is mainly because local sections of rings unfold and become more and more similar to the same section of a linear chain for increasing N . The fraction of the inner area $A(r_b > 2)$ in Figure 7 fits well against $\sim N^{1/2}(1 - P_{OO})$ using the non-concatenation probability $P_{OO} = \exp(-(N - a)/N_{OO})$ with $a = 15.0 \pm 0.5$ and $N_{OO} = 40.0 \pm 0.2$ at $\phi = 0.5$, as described in ref. [1]. Thus, the data on the exponential tail and the data on the number of linked rings f_n of ref. [1] agree well with each other. The fact that the compression of rings is only driven by the changes in the inner area is demonstrated by comparing with the inner area of entangled rings: the area fractions at $r_b < 2$ are the same in both cases, which is exemplified here by comparing with the non-constant fraction $A(1 < r_b < 2)$, but the inner

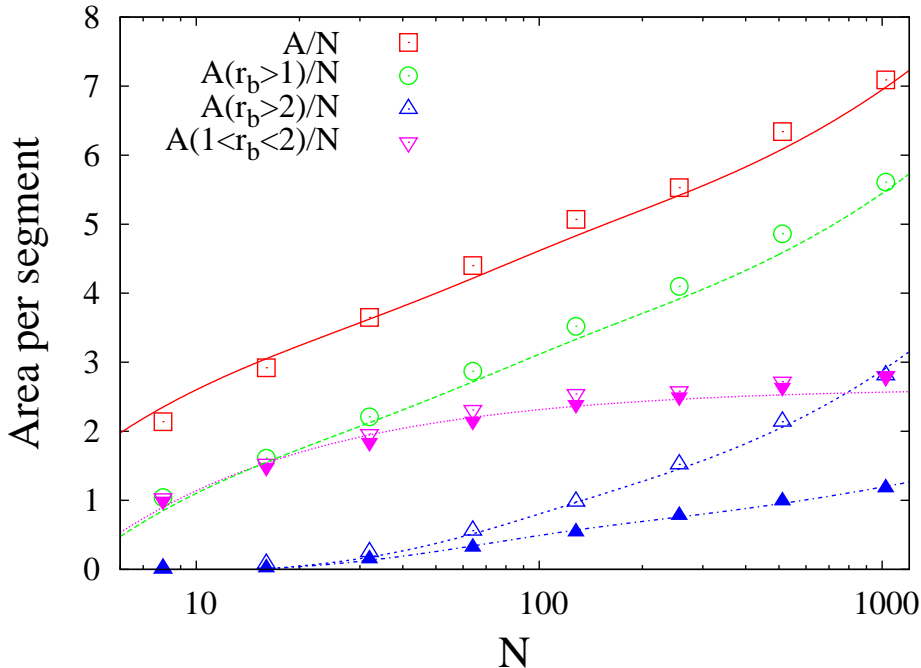


Figure 7: Total area per bond A/N (measured in square lattice units) and the area fraction $A(r_b > 1)/N$ with its contributions close to the boundary $A(1 < r_b < 2)/N$ and further away from the boundary $A(r_b > 2)/N$ in comparison. Open symbols is data of interpenetrating rings, full symbols additional data of entangled rings.

part of the area is clearly reduced following a dependence $\sim N^{1/3}(1 - P_{OO})$.

It is quite interesting to note that even for the largest N the inner fraction of the area is still not the largest part of the minimal area. When extrapolating the data, inner area and boundary become comparable in the range of the knotting length N_0 of these samples [1]. Knotting as well as linking other rings requires an open area that can be penetrated by a strand of the same polymer (knotting) or different polymer (linking). Therefore, it might be an interesting subject for a future study to compare knotting of individual rings of variable excluded volume with the change in the inner minimal area of ring polymers.

4 Internal structure of ring polymers in a melt

The models of Lang *et al.* [1], Cates and Deutsch [6], and Sakaue [3, 7] differ clearly in their predictions or assumptions on the microscopic structure of rings in a melt of rings. Sakaue [3, 7] postulates a change in the topological length scale as function of melt molecular weight. Thus, local conformations of rings are expected to be a function of melt molecular weight. In particular, the onset of compression is expected to move to smaller distances in space and along the chains with increasing M .

Cates and Deutsch do not discuss the bidisperse case, however, a generalization of scaling to

bidisperse blends is straight forward. The size of swollen rings in good solvent is fixed at $R_s \sim M^{-1/5}N^{3/5}$ and in monodisperse melts $R_m \sim N^{2/5}$. We further note that in the approach of Cates and Deutsch and, thus, in equation (3), only R , N , and M enter. Therefore, there are no other physical length scales in this model and any cross-over can only be a function of these variables. Searching for the cross-over point we find $M_c = N$, which is also the limiting case under which such a scaling could be applied. Thus, the only possible scaling of ring conformations in bidisperse melts consistent with the Cates and Deutsch conjecture is

$$R \sim M^{-1/5}N^{3/5} \quad (5)$$

for $M \leq N$ and

$$R \sim N^{2/5} \quad (6)$$

for $M > N$. On a microscopic level, this is consistent with rings that are compressed on local scale comparable to the size of the surrounding rings while staying ideal on larger length scales. Furthermore, rings are expected to be ideal for $M_c = N^{1/2}$ and thus, the onset of compression is expected to be a function of N independent of the entanglement degree of polymerization N_e of the polymers.

The model of Lang *et al.* [1] makes the following assumptions or predictions: a) the compression of rings in melt is related to the number of overlapping rings that would be mutually concatenated. b) The topological length scale (entanglement length) is constant. The onset of compression is controlled by the onset of mutual penetration of rings at N_{OO} . c) Since the rings adopt conformations that are subject to minimizing the bounded area, a significant increase of the fraction double folded ring sections can be expected. These folds could become visible as an anti-correlation peak in the bond-bond correlation function.

The different predictions or assumptions of the models above are now tested in detail. Let us first treat ideal rings of N monomers as basis for our discussion. Let $1 \leq S \leq N/2$ denote the minimum number of segments between monomer i and j along the ring. The two strands of S and $N - S$ connecting monomer i and j act like an elastic chain of length

$$s = \frac{S(N - S)}{N} \quad (7)$$

connecting both monomers. The average distance between monomer i and j in an ideal ring is therefore

$$R_e(s) = bs^{1/2}. \quad (8)$$

Wittmer *et al.* [2, 10] reported corrections to the ideal behaviour for linear chains in melt, which result in long range bond correlations and a slow convergence of chain size towards the asymptotic limit. This slow convergence is visible as correction to the average root mean square distance between to monomers along a linear chain. As shown in Figure 8, the smallest s contribute most of this correction for linear chains. Obviously, $s = S$ for linear chains. For long rings $N \gg 1$ there

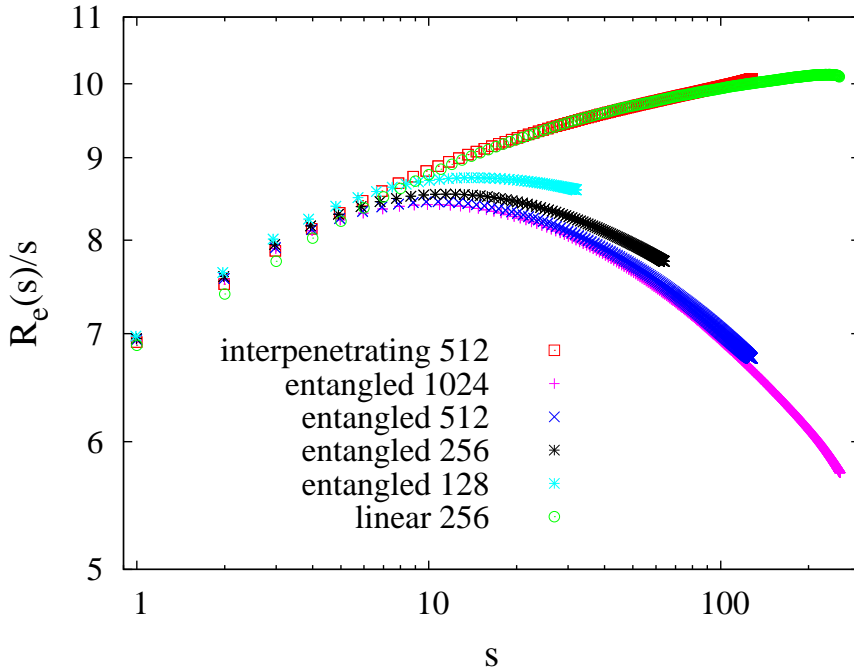


Figure 8: Normalized mean square distance between monomers separated by an elastic strand of s segments in monodisperse melts.

is $s \approx S$ at small S . Therefore, we do not expect large deviations between long linear chains in melts and long interpenetrating rings that are not affected by entanglements. This is demonstrated by the excellent overlap of the data of interpenetrating rings and linear chains in Figure 8 when plotting $R_e(s)$ as function of s both times. This overlap further shows that our samples were well equilibrated and the low scatter of the data (which is in fact the correction to scaling of ring size) indicates the high precision of the results. Note that switching off entanglements (see section 2) increases the average square bond length from 6.95 to 7.45 due to the modification of the set of bond vectors. Overlap of the data was thus obtained by renormalizing size by the change in the average square bond length of the interpenetrating rings.

The data of the entangled ring samples shows a clearly different behaviour in Figure 8, whereby the sample with $N = 128$ is at the onset of the fully entangled regime (cf. below). For larger rings, at $s \approx 10$, the tangent to the mean square distance becomes horizontal indicating that the remaining effect of excluded volume is fully compensated by topological interactions. For larger s , rings become increasingly compressed with increasing s , whereby the data of large N appear to fall on a rather universal curve. The short distance behaviour is nearly unaffected. This observation is clearly different to the model of Sakaue [3, 7], which postulates a change in the topological length scale as function of melt molecular weight. A change in the topological length scale should lead to a shift of the peak position as function of s . Such a behaviour cannot be deduced from Figure 8. Similarly, the extended model of Cates and Deutsch would also predict a shift of the onset of compression as function of $M \sim N^{1/2}$. This is not supported by Figure 8.

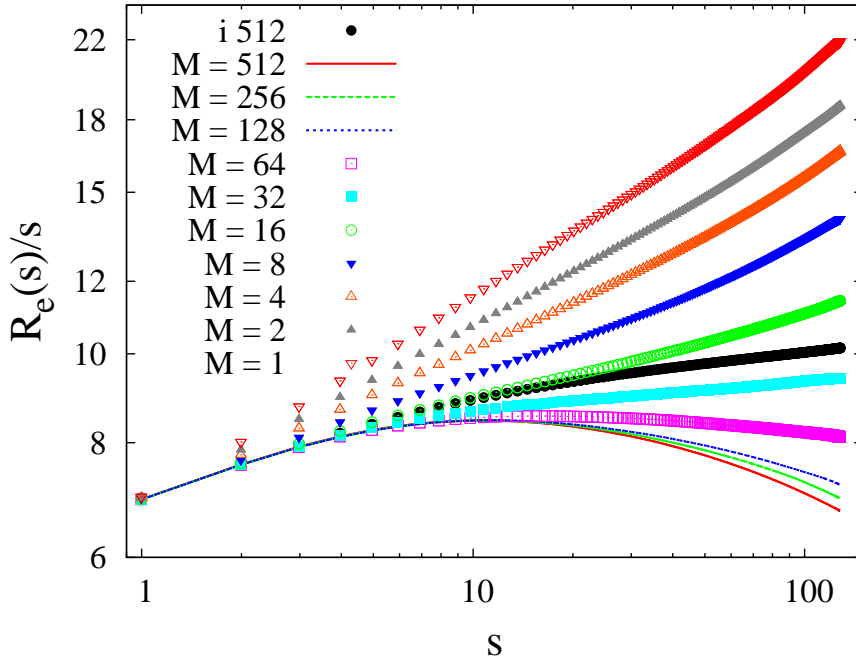


Figure 9: Normalized mean square distance between monomers separated by an elastic strand of s segments. Data of entangled rings of $N = 512$ are shown as function of the degree of polymerization M of the surrounding melt of entangled rings (and in melts of short linear chains for $M \leq 2$). The monodisperse sample $N = 512$ of interpenetrating rings (sample i 512) is included for comparison.

It is worth pointing out that even though the rings are compressed as compared to their linear counterparts, this compression is still so small that rings up to $N \approx 500$ monomers are slightly swollen in Figure 8 as compared to ideal rings. This can be seen from $R_e(s)/s > R_e(1)$, since for ideal rings $R_e(s)/s \equiv R_e(1)$.

The internal distances inside the rings are analyzed as function of melt molecular weight, see Figure 9. Again, the deviation from the monodisperse case $M = 512$ starts at large distances, whereby short distances are nearly unaffected. For $M \leq 16$, which is equivalent to $M < N^{1/2}$, the ring conformations are additionally affected by swelling (as compared to the monodisperse reference sample $N = 512$ of interpenetrating rings) due to low molecular weight solvent. This type of swelling manifests itself in parallel sets of data at large s for decreasing M , since the onset of swelling further propagates to smaller s . The compression of rings with $M \geq 32$ is qualitatively different, since the data at large s is no longer parallel.

Wittmer et al. [2, 10] identified time average bond-bond correlations $\langle \mathbf{b}_j, \mathbf{b}_i \rangle$ as source of changes in the internal distances $R_e(s)$. Let the vector \mathbf{r}_j denote the coordinates of monomer j and $\mathbf{b}_j = \mathbf{r}_{j+1} - \mathbf{r}_j$ the bond vector connecting monomer j and $j + 1$. Note that rings are “periodic” in the sense that $\mathbf{r}_{N+i} = \mathbf{r}_i$. Furthermore, ring closure is expressed by $\sum_{i=1}^N \mathbf{b}_i = \mathbf{0}$. This condition implies $\sum_i \langle \mathbf{b}_j, \mathbf{b}_i \rangle = 0$ and $\mathbf{b}_i = -\sum_{j \neq i} \mathbf{b}_j$. Due to $\langle \mathbf{b}_i, \mathbf{b}_i \rangle = b^2$ for any i with root mean square

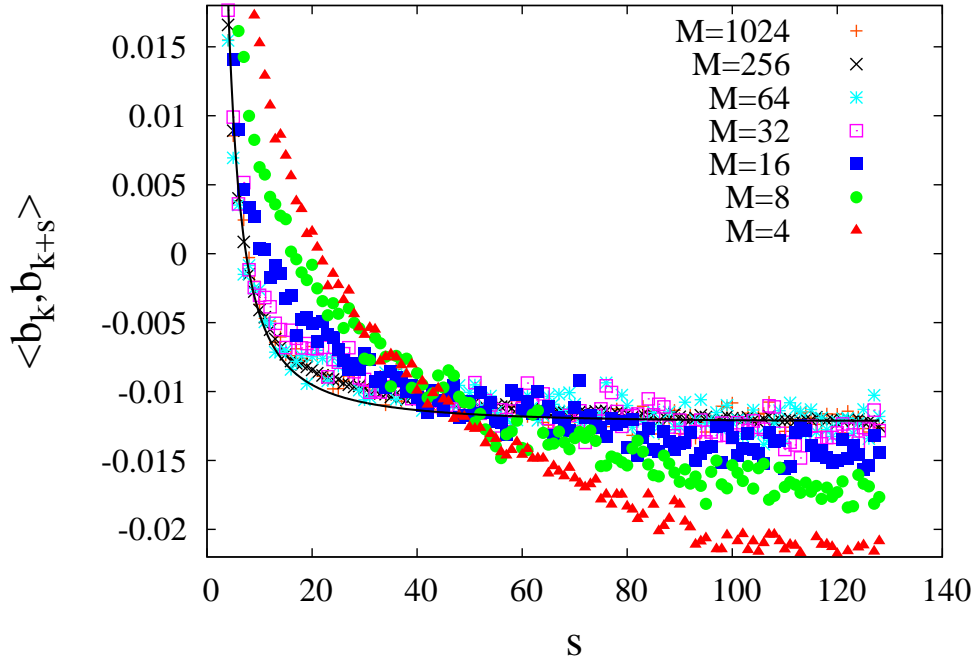


Figure 10: Bond correlations in a melt of interpenetrating rings of M monomers as experienced by rings with $N = 256$. The line is a fit to the data $M = 256$ as described in the text.

bond length b we thus have the average correlation

$$\langle \mathbf{b}_j, \mathbf{b}_i \rangle = -b^2/(N - 1) \quad (9)$$

among two bonds $i \neq j$ in an ideal ring.

Excluded volume interactions introduce long range bond-bond correlations that decay as a power law [2, 10]. These correlations lead to a renormalization of the effective bond length in melt, such that the chain conformations can be described by a random walk with an effective bond length $b_e \approx 1.23b$ at $\phi = 0.5$ in the limit of large N . For very large rings with excluded volume we, thus, expect that the bond-bond correlation function $\langle \mathbf{b}_j, \mathbf{b}_{j+S} \rangle$ drops from the linear chain power law $S^{-3/2}$ in a melt of long rings at small S to approximately $\langle \mathbf{b}_j, \mathbf{b}_{j+S} \rangle \approx -b_e^2/(N - 1)$ for $S \approx N/2$. Fitting the monodisperse melt data of $M = 256$ with $\langle \mathbf{b}_j, \mathbf{b}_{j+S} \rangle = \text{const} \cdot S^{-3/2} - b_e^2/(N - 1)$ in Figure 11 (black line) yields reasonable agreement supporting this simple approximate treatment. The data further show that bond correlations become universal in melts $M \gtrsim N^{1/2}$.

The same analysis for the entangled samples yields a clearly different result. For sufficiently large N , an anti-correlation peak is formed around $S \approx 10$ in Figure 11 for increasing melt degree of polymerization M . A similar anti-correlation has been observed previously in monodisperse melts of rings [17]. Peak position and amplitude become independent of melt molecular weight for $M \geq 128$ similar to the position of the maximum in Figure 9. The anti-correlation peak also leads to a reduction of anti-correlation at large S .

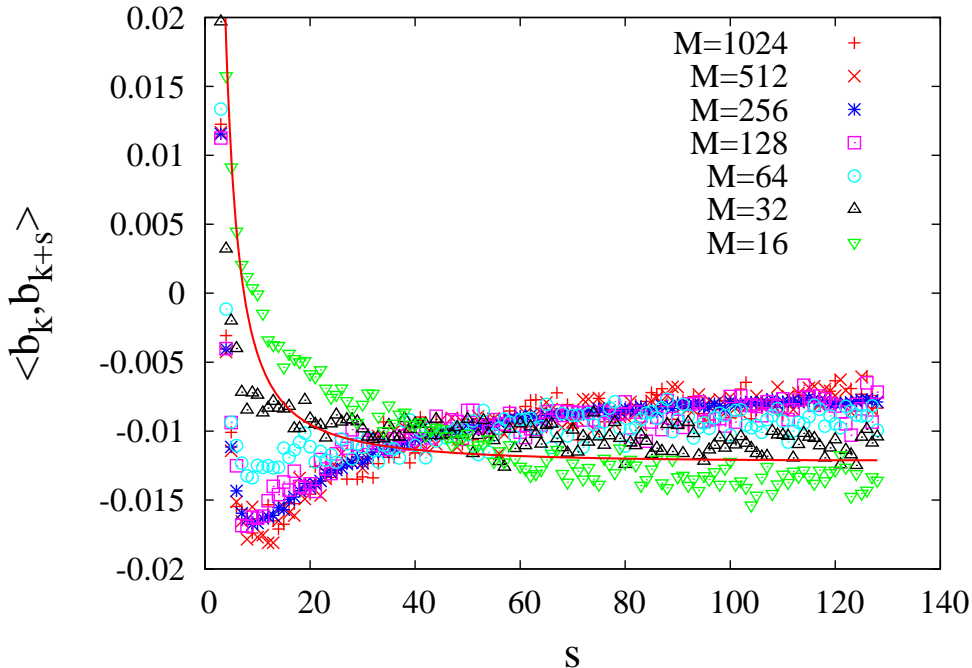


Figure 11: Bond correlations in entangled melts of rings for $N = 256$. The line is the same approximation as used for the unentangled data Figure 11 for comparison.

Both observations (anti-correlation and maximum in normalized internal distances) could be explained, if the rings contain a significant amount of short double folded sections of about 10 monomers. The formation of such double folds, however, requires that topology is important for short strands (of long rings) at about 10 monomers. Note that an onset of entanglement effects at the same $s \approx 10$ was found in a recent work on networks [18]. As mentioned above, Sakaue [3, 7] postulates a shift of the topological length scale as function of M . Also, the CD model requires the onset of compression to be $\sim M^{1/2}$. This is in clear disagreement to the constant peak position in Figure 11 for sufficiently large M .

5 Size of dilute N -mer rings in melts of M -mer rings: a comparison of entangled and interpenetrating rings

In order to subtract the effect of excluded volume swelling from ring compression, the ratio of the sizes of rings in the interpenetrating and the entangled samples, R_{in}/R_{en} , is analyzed. The result is taken to power 5/2, since then, all corrections to the first term of the free energy in equation (1) show up in first power. In ref [1] it was shown that the predominant correction at small N should be a cut-off for non-concatenation of form $P_{OO} = \exp(-(N - a)/N_{OO})$. This cut-off was determined in monodisperse melts. For an N -mer ring in a melt of M -mer rings, the cut-off is controlled by the M -mer rings, if $N > M$. Therefore, we have to plot the data as function of M and use a function of form $P_{OO}(M) = \exp(-(M - a^*)/N_{OO})$ to describe the onset of concatenation, and thus, compression of

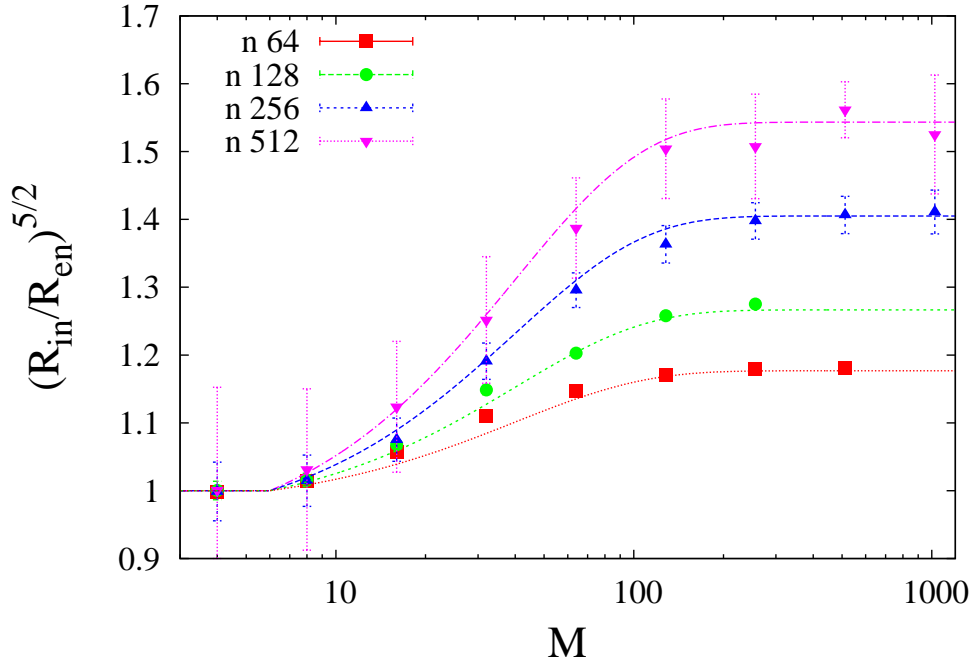


Figure 12: Size of interpenetrating rings normalized by the size of entangled rings.

the N -mer. No further changes in ring size are expected in melts of sufficiently large $M > N_{OO}$ beyond the cut-off N_{OO} and the cut-off N_{OO} itself should remain unaffected for $N > N_{OO}$. As compared to the monodisperse case, the onset of compression as modeled by parameter a might be reduced for large N -mers in a melt of M -mers, since now only the smaller M -mer requires to locally unfold to allow for penetration. Therefore, a^* was introduced as adjustable parameter and it was found that the data at small M is best approximated for an $a^* \approx a/2$ when being compared with the monodisperse a .

Figure 12 compares the $(R_{in}/R_{en})^{5/2}$ and the onset of compression towards larger M with a function of form $const \cdot (1 - P_{OO}) + 1$. The good agreement of the onset of compression with this function shows that the correction P_{OO} is the dominating correction for the onset of ring compression in bidisperse blends. The plateau at large M demonstrates that ring size is approximately constant in melts of larger degree of polymerization, at least for the range of $100 \lesssim N \lesssim 1000$, as accessible in the present study. This is because the exponential decay of the distribution of inner areas suppresses further corrections as function of M for the rather small ratio of N/M available with $N, M > N_{OO}$ and $N, M \lesssim 1000$. Obviously, the level of the plateau for compression at $N \geq 128$ is in agreement with a scaling of ring size $\sim N^{2/5}$, since the plateau is mainly reached for $M \geq 128$ and the corresponding sizes of rings in monodisperse samples scale as $R \sim N^{2/5}$, as discussed previously in ref [1].

It will be very interesting to repeat the present analysis for bidisperse blends of rings of clearly larger size such that the ratio of N/M eventually becomes sufficient to change the plateau as function of M into an increasing function of M . If the analysis of ref. [1] for larger N is correct, there will be

even more interesting modifications to the behaviour at large N and M . First, if ring compression is sufficiently large, $N > N_C$, a non-knotting contribution N^3/R^6 is balancing non-concatenation. For such N , a different scaling of the plateau level should be observed in Figure 12. Next, above a critical N^* essentially any pair of overlapping rings should be entangled. Then, compression should become a function of M for sufficiently large N , $M > N^*$ while remaining constant (beyond $N > N_{OO}$ and up to the corrections mentioned above) for $N < N^*$.

6 Summary

Ring conformations in entangled and interpenetrating melts were compared in the present work. To understand the compression of the entangled rings, the minimal area bounded by the ring contour is analyzed. It is found that the area distribution of rings is decaying exponentially as function of $(r_b - r_c)/N^\alpha$, whereby r_b is the distance of the center of an area segment to the nearest monomer of the ring, r_c is a geometrical cut-off related to bead diameter, and N is the degree of polymerization of the ring. The characteristic exponent is $\alpha \approx 0.588$ for swollen rings, $\alpha \approx 1/2$ for unentangled interpenetrating rings, and $\alpha \approx 1/3$ for entangled rings. The N -dependence of the exponential decay leads to a correction $\sim N^\alpha$ to the minimal area bounded by a ring polymer. For interpenetrating rings, this leads to a number of rings that have to be expelled in case of monodisperse entangled melts $\sim \phi R^2$, as found previously in ref. [1]. The results of section 3 demonstrate that only the inner fraction of the area that is subject to penetrations is getting modified upon compression of ring polymers in melts or swelling of rings in low molecular weight solvents.

The internal structure of entangled rings was analyzed to test the applicability of the models available in literature [1, 3, 6, 7]. An extension of the model of Cates and Deutsch [6] leads to an onset of compression in melts with melt degree of polymerization $M \sim N^{1/2}$, which is not confirmed by the simulation data of the present study. The model of Sakaue [3, 7] assumes that the topological length scale becomes a decreasing function for increasing M . The model of Lang et al. [1] requires a constant entanglement length and uses an exponential cut-off for the entanglement effects towards small M . After this onset, the effect of entanglements is assumed to be constant. The former two models should manifest themselves in a change of the internal structure of the rings that is a function of melt molecular weight. The simulation data of the present study agree only with the model of ref [1]: for sufficiently large M there is a broad range of melt molecular weights with constant peak positions in the normalized mean square internal distances $R_e(s)/s$ or in the bond-bond correlation function. Both peaks arise only for entangled samples and are absent in interpenetrating samples. Thus, we have to conclude that these peaks must be related to entanglements between the rings. In consequence, the length scale of topological interactions (entanglement length) in a melt of entangled rings must be constant in contrast to the recent proposal by Sakaue [3]. This observation is corroborated by a comparison of ring sizes in entangled and interpenetrating melts, which shows that the ring size remains constant as soon as the concatenation probability converges to one.

7 Acknowledgement

The author is indebted to J.-U. Sommer, J. Fischer, T. Kreer, and M. Rubinstein for stimulating discussions on this subject and the author thanks the DFG for funding grant LA2375/2-1 and the ZIH Dresden for a generous grant of computing time under the project BiBPoDiA.

References

- [1] Lang, M.; Fischer, J.; Sommer, J.-U. *Macromolecules* **2012**, *45*, 7642–7648.
- [2] Wittmer, J. P.; Beckrich, P.; Meyer, H.; Cavallo, A.; Johner, A.; Baschnagel, J. *Phys. Rev. E* **2007**, *76*, 11803.
- [3] Sakaue, T. *Phys. Rev. E* **2012**, *85*, 021806.
- [4] Moore, N. T.; Grosberg, A. Y. *J. Phys. A* **2006**, *39*, 9081–9092.
- [5] Grosberg, A. Y.; Feigel, A.; Rabin, Y. *Phys. Rev. E* **1996**, *54*, 6618–6622.
- [6] Cates, M. E.; Deutsch, J. M. *J. de Physique* **1986**, *47*, 2121–2128.
- [7] Sakaue, T. *Phys. Rev. Lett.* **2011**, *106*, 167802.
- [8] de Gennes, P. G. *Scaling Concepts In Polymer Physics*; Cornell University Press: New York, NY, 1991.
- [9] Rubinstein, M.; Colby, R. *Polymer Physics*; Oxford University Press: New York, NY, 2003.
- [10] Wittmer, J. P.; Meyer, H.; Baschnagel, J.; Johner, A.; Obukhov, S.; Mattioni, L.; Müller, M.; Semenov, A. N. *Phys. Rev. Lett* **2004**, *93*, 147801.
- [11] Carmesin, I.; Kremer, K. *Macromolecules* **1988**, *21*, 2819–2823.
- [12] Michalke, W.; Lang, M.; Kreitmeier, S.; Göritz, D. *Phys. Rev. E* **2001**, *64*, 012801.
- [13] Edwards, M.; Doi, S. *The Theory Of Polymer Dynamics*; Oxford University Press: New York, NY, United States of America, 1986.
- [14] Adams, C. C. *Das Knotenbuch: Einführung in die mathematische Theorie*; Spektrum akademischer Verlag: Heidelberg, 1995.
- [15] Metropolis, N.; Rosenbluth, A.; Rosenbluth, M.; Teller, A.; Teller, E. *J. Chem. Phys.* **1953**, *21*, 1087–1092.
- [16] Clisby, N. *Phys. Rev. Lett.* **2010**, *104*, 055702.
- [17] Müller, M.; Wittmer, J. P.; Cates, M. E. *Phys Rev E* **2000**, *61*, 4078–4089.
- [18] Lang, M.; Sommer, J.-U. *Phys. Rev. Lett.* **2010**, *104*, 177801.

Table of Contents Graphic

Minimal surface bounded by polymer rings: normalized distribution of area segments as function of the distance r_b to the boundary

Michael Lang

